INTERNATIONAL JOURNAL FOR NUMERICAL METHODS IN ENGINEERING
Int. J. Numer. Meth. Engng 2003; **56**:1375–1396 (DOI: 10.1002/nme.612)

On a new integration scheme for von-Mises plasticity with linear hardening

Ferdinando Auricchio[1,2,*,†] and Lourenço Beirão da Veiga[3]

[1]*Dipartimento di Meccanica Strutturale, Università di Pavia, Via Ferrata 1, 27100 Pavia, Italy*
[2]*Istituto di Matematica Applicata e Tecnologie Informatiche, CNR, Pavia, Italy*
[3]*Dipartimento di Matematica, Università di Pavia, Via Ferrata 1, 27100 Pavia, Italy*

SUMMARY

Limiting the discussion to an associative von-Mises plasticity model with linear kinematic and isotropic hardening, we compare the performance of the classical radial return map algorithm with a new integration scheme based on the computation of an integration factor. The numerical examples clearly show the improved accuracy of the new method. Copyright © 2003 John Wiley & Sons, Ltd.

KEY WORDS: plasticity; numerical integration algorithm; return map; exact integration; integration factor

1. INTRODUCTION

The numerical solution of non-linear inelastic models is a topic of wide scientific interest due to the need of accurately reproducing the constitutive response of real materials in computational enviroments (such as commercial finite element codes).

Limiting ourselves to the simple case of an associative von-Mises elasto-plastic material model with linear kinematic and isotropic hardening, in the present paper we compare a new numerical scheme based on the computation of a model integration factor with the well established and performing *radial return map* algorithm. In fact, motivated by a work recently proposed in the literature [1, 2], the numerical solution obtained with the new method is exact in the case of a material with a linear kinematic hardening, approximated in the case of a material with isotropic or mixed hardening.

After a brief review of the return map method for the model under investigation, we present in detail the new method theoretical background and numerical procedure, addressing also the computation of the algorithmically consistent tangent matrix. We then compare the numerical accuracy of the two schemes for different stress–strain load histories as well for an initial boundary value problem.

* Correspondence to: Ferdinando Auricchio, Dipartimento di Meccanica Strutturale, Università di Pavia, Via Ferrata 1, 27100 Pavia, Italy
† E-mail: auricchio@unipv.it

Received 18 September 2001
Revised 22 May 2002
Accepted 22 May 2002

The numerical tests show the improved performance of the new method; moreover, the new method shows a quadratic error convergence in relation to the discrete time interval length, while the return map shows a linear behaviour.

We conclude the paper with the appendix, pointing out differences and similarities between the method here presented and other methods available in the literature and also based on an exact model integration [3–7].

2. TIME CONTINUOUS MODEL

We consider an *associative von-Mises plasticity model with linear kinematic and isotropic hardening* in the realm of small deformations (refer for example to References [8] or [9]). Introducing a linear isotropic elastic relation, the volumetric plastic strain is zero, leading to a deviatoric–volumetric decoupling. Therefore, it is convenient to split the strain and stress tensors, $\boldsymbol{\sigma}$ and $\boldsymbol{\varepsilon}$, as

$$\boldsymbol{\sigma} = \mathbf{s} + p\mathbf{1} \quad \text{with } p = \tfrac{1}{3}\mathrm{tr}(\boldsymbol{\sigma}) \tag{1}$$

$$\boldsymbol{\varepsilon} = \mathbf{e} + \tfrac{1}{3}\theta\mathbf{1} \quad \text{with } \theta = \mathrm{tr}(\boldsymbol{\varepsilon}) \tag{2}$$

The equations for the model are

$$p = K\theta \tag{3}$$

$$\mathbf{s} = 2G[\mathbf{e} - \mathbf{e}^p] \tag{4}$$

$$\boldsymbol{\Sigma} = \mathbf{s} - \boldsymbol{\alpha} \tag{5}$$

$$F = \|\boldsymbol{\Sigma}\| - \sigma_y \tag{6}$$

$$\dot{\mathbf{e}}^p = \dot{\gamma}\mathbf{n} \tag{7}$$

$$\sigma_y = \sigma_{y,0} + H_{\mathrm{iso}}\gamma \tag{8}$$

$$\dot{\boldsymbol{\alpha}} = H_{\mathrm{kin}}\dot{\mathbf{e}}^p \tag{9}$$

$$\dot{\gamma} \geqslant 0, \quad F \leqslant 0, \quad \dot{\gamma}F = 0 \tag{10}$$

where

- Equation (3) represents the volumetric elastic relation, with K the material bulk modulus and θ the total volumetric strain.
- Equation (4) represents the deviatoric elastic relation with G the material shear modulus, $\mathbf{e}$ the total deviatoric strain, $\mathbf{e}^p$ the traceless plastic strain, and where we use the standard additive decomposition of the strain $\mathbf{e} = \mathbf{e}^e + \mathbf{e}^p$.
- Equation (5) introduces the *relative stress* $\boldsymbol{\Sigma}$ in terms of the *backstress* $\boldsymbol{\alpha}$, introduced to describe a kinematic hardening mechanism.

- Equation (6) is the von Mises yield function, expressed in terms of the relative stress $\boldsymbol{\Sigma}$, where $\|\bullet\|$ is the euclidean norm and σ_y the yield stress.
- Equation (7) determines the evolution of the plastic strain, where γ is a scalar quantity known as *consistency parameter*, the superposed dot indicates a time derivative, while $\mathbf{n}$ is defined as

$$\mathbf{n} = \frac{\partial F}{\partial \boldsymbol{\Sigma}} = \frac{\boldsymbol{\Sigma}}{\|\boldsymbol{\Sigma}\|} \tag{11}$$

- Equation (8) represents a linear isotropic hardening mechanism, governing the radius of the yield surface $F = 0$. In particular $\sigma_{y,0}$ is the initial yield stress and H_{iso} is a material constant.
- Equation (9) represents a linear kinematic hardening mechanism, governing the evolution of the backstress $\boldsymbol{\alpha}$, hence the shift of the yield function in the stress space.
- Equations (10) are the Kuhn-Tucker conditions. In particular, the second equation limit the relative stress within the boundary defined by the yield surface $F = 0$, while the other two are necessary to determine the plastic strain behaviour. With a slight oversimplification of the model complexity, we may say that when $\dot{\gamma} = 0$ the system is in an *elastic phase*, while when $\dot{\gamma} > 0$ we say that the system is in a *plastic phase*.

Remark 1
We observe that, due to its simple linear behaviour, finding the exact solution of the volumetric part is immediate; therefore, in the sequel we treat only the more interesting deviatoric part of the model.

Remark 2
In the present work, we consider all second-order tensors as 9-component column vectors; this is done ordering the tensor components in a vector format. This formal modification simplifies the descriptive and the numerical parts of the work. Clearly, due to the symmetry of the second-order tensors involved, the numerical implementation of both algorithms is done using only 6-component vectors.

3. RADIAL RETURN MAP

We now briefly review a numerical method often used to approach the solution of the described plasticity model, the *radial return map*, in the following also indicated simply as *return map*. A more detailed description can be found in several articles and books [10–13]; it is anyway worth recalling here the widespread success of such a method, granted by its general good numerical performances and the well-established numerical properties. In general, the method consists in:

1. the time-integration of the differential algebraic system, leading to an algebraic system;
2. the formulation of the solution algorithm for the obtained algebraic system.

In particular, for the simple model under investigation, adopting a first-order Backward Euler time integration formula, the solution of the algebraic system returns a simple linear equation

and, accordingly, the solution algorithm reduces to a radial return map. In the following, we briefly review the method together with the form of the consistent tangent.

Problem integration: We start assuming that the load history interval $[0, T]$ is divided into N sub-intervals defined by the points $0 = t_0 < t_1 < \cdots < t_n < t_{n+1} < \cdots < t_N < t_{N+1}$. If t_n is a generic time instant, we indicate by $\mathbf{e}_n$ the deviatoric strain at time t_n, by $\mathbf{s}_n$ the deviatoric stress at the same time, and so on for all the problem variables.

As for most numerical schemes built to solve a constitutive equation, we suppose that the strain history path is known (strain driven problem); we are then interested in the evolution of the other problem variables, in particular the stress, the plastic strain and the total strain.

As an example, assuming to know the values $(\mathbf{s}_n, \mathbf{e}_n, \gamma_n, \boldsymbol{\alpha}_n)$ at time t_n, and the deviatoric strain $\mathbf{e}_{n+1}$ at time t_{n+1}, we search for the remaining variables at time t_{n+1}.

To solve the problem, we initially suppose the step to be elastic, and calculate the trial values:

$$\begin{aligned} \mathbf{e}_{n+1}^{p,TR} &= \mathbf{e}_n^p \\ \mathbf{s}_{n+1}^{TR} &= 2G[\mathbf{e}_{n+1} - \mathbf{e}_n^p] \\ \boldsymbol{\alpha}_{n+1}^{TR} &= \boldsymbol{\alpha}_n \\ \boldsymbol{\Sigma}_{n+1}^{TR} &= \mathbf{s}_{n+1}^{TR} - \boldsymbol{\alpha}_{n+1}^{TR} \\ \gamma_{n+1}^{TR} &= \gamma_n \end{aligned} \tag{12}$$

If the resulting stress is admissible, i.e.

$$\|\boldsymbol{\Sigma}_{n+1}^{TR}\| \leqslant \sigma_{y,0} + H_{\text{iso}}\gamma_{n+1}^{TR} \tag{13}$$

the variable values at the time step t_{n+1} are taken as the trial ones just calculated. On the other hand, if $\boldsymbol{\Sigma}_{n+1}^{TR}$ violates the yield limit (13), a plastic correction is introduced

$$\begin{aligned} \mathbf{e}_{n+1}^{p} &= \mathbf{e}_{n+1}^{p,TR} + \lambda\mathbf{n} \\ \mathbf{s}_{n+1} &= \mathbf{s}_{n+1}^{TR} - 2G\lambda\mathbf{n} \\ \boldsymbol{\alpha}_{n+1} &= \boldsymbol{\alpha}_{n+1}^{TR} + H_{\text{kin}}\lambda\mathbf{n} \\ \boldsymbol{\Sigma}_{n+1} &= \boldsymbol{\Sigma}_{n+1}^{TR} - [2G + H_{\text{kin}}]\lambda\mathbf{n} \\ \gamma_{n+1} &= \gamma_{n+1}^{TR} + \lambda \end{aligned} \tag{14}$$

where the scalar λ represents the increment of the plastic consistency parameter i.e. $\int_{t_n}^{t_{n+1}} \dot{\gamma}\, \mathrm{d}t$.

Algebraic solution: The solution of the obtained algebraic system is approached solving initially for the scalar λ, enforcing the condition $F(\boldsymbol{\Sigma}) = 0$. This implicit equation is solved observing that $\boldsymbol{\Sigma}_{n+1}^{TR}$ and $\boldsymbol{\Sigma}_{n+1}$ are parallel, obtaining

$$\lambda = \frac{\|\boldsymbol{\Sigma}_{n+1}^{TR}\| - (\sigma_{y,0} + H_{\text{iso}}\gamma_{n+1}^{TR})}{2G + H_{\text{iso}} + H_{\text{kin}}} \tag{15}$$

Once the scalar λ is known, noting that

$$\mathbf{n}^{TR} = \frac{\boldsymbol{\Sigma}_{n+1}^{TR}}{\|\boldsymbol{\Sigma}_{n+1}^{TR}\|} = \mathbf{n} \tag{16}$$

it is possible to update all the problem variables.

Tangent matrix: The algorithmically consistent tangent matrix is obtained linearizing the time-discrete algorithmic procedure. In particular, for a plastic step (i.e. such that $\lambda \neq 0$), we get

$$\mathbb{D}_{\text{disc}} = K(\mathbf{i}\,\mathbf{i}^{\mathrm{T}}) + 2G(1-C)\mathbb{I}_{\text{dev}} + [2G(C-A)]\mathbf{n}^{TR}[\mathbf{n}^{TR}]^{\mathrm{T}} \tag{17}$$

where $\mathbf{i}$ is the vector corresponding to the second-order identity tensor, the superscript T indicates the transpose and

$$A = \frac{2G}{2G + H_{\text{iso}} + H_{\text{kin}}} \tag{18}$$

$$C = \frac{2G\lambda}{\|\boldsymbol{\Sigma}_{n+1}^{TR}\|} \tag{19}$$

$$\mathbb{I}_{\text{dev}} = \mathbb{I} - \tfrac{1}{3}\mathbf{i}\,\mathbf{i}^{\mathrm{T}} \tag{20}$$

$\mathbb{I}$ being the identity matrix. The calculation of $\mathbb{D}_{\text{disc}}$ hides no particular difficulties and details can be found for example in Reference [12].

4. DIFFERENT MODEL FORMULATION

Before addressing the new integration scheme, we need to convert the original differential problem in a different but equivalent one.

In fact, as noted in the literature [1, 2], an associative von-Mises plasticity model with linear kinematic hardening can be formulated as a differential problem of the following type:

$$\dot{\mathbf{X}} = \mathbb{A}\mathbf{X} \tag{21}$$

with the matrix $\mathbb{A}$ constant both in the elastic and in the plastic phase. Remarkably, this is a linear problem with a well-known solution.

Accordingly, the goal of the present section is to propose a clean construction for the model re-formulation in the format of Equation (21) and to extend such an approach to the more general case of associative von-Mises plasticity model with combined kinematic and isotropic hardening. For combined kinematic and isotropic hardening the obtained differential problem remains of type (21), but with $\mathbb{A}$ 'slightly' dependent on $\mathbf{X}$. Therefore, in such a case, we will apply a numerical scheme to solve our dynamical system (21).

Formulation (21) is obtained as follows. Combining Equations (4) and (5), we obtain

$$\boldsymbol{\Sigma} + \boldsymbol{\alpha} + 2G\mathbf{e}^{p} = 2G\mathbf{e} \tag{22}$$

and, taking the derivative in time and applying Equation (9), Equation (22) becomes

$$\dot{\boldsymbol{\Sigma}} + (2G + H_{\text{kin}})\dot{\mathbf{e}}^p = 2G\dot{\mathbf{e}} \tag{23}$$

Now, recalling that in the plastic phase

$$\mathbf{n} = \frac{\boldsymbol{\Sigma}}{\|\boldsymbol{\Sigma}\|} = \frac{\boldsymbol{\Sigma}}{\sigma_{y,0} + H_{\text{iso}}\gamma} \tag{24}$$

we may apply (7) obtaining

$$\dot{\boldsymbol{\Sigma}} + (2G + H_{\text{kin}})\frac{\boldsymbol{\Sigma}}{\sigma_{y,0} + H_{\text{iso}}\gamma}\dot{\gamma} = 2G\dot{\mathbf{e}} \tag{25}$$

which is a differential equation for $\boldsymbol{\Sigma}$. We now need an evolution law for γ, which in the elastic phase is simply

$$\dot{\gamma} = 0 \tag{26}$$

while in the plastic phase it is indirectly extracted from the Kuhn–Tucker condition $\dot{F} = 0$. Multiplying (scalar product) Equation (25) by $\boldsymbol{\Sigma}$ it follows

$$\boldsymbol{\Sigma}^{\mathrm{T}}\dot{\boldsymbol{\Sigma}} + (2G + H_{\text{kin}})\frac{\|\boldsymbol{\Sigma}\|^2}{\sigma_{y,0} + H_{\text{iso}}\gamma}\dot{\gamma} = 2G[\dot{\mathbf{e}}^{\mathrm{T}}\ \boldsymbol{\Sigma}] \tag{27}$$

and, observing that in the plastic phase

$$\|\boldsymbol{\Sigma}\|^2 = (\sigma_{y,0} + H_{\text{iso}}\gamma)^2 \tag{28}$$

$$\boldsymbol{\Sigma}^{\mathrm{T}}\dot{\boldsymbol{\Sigma}} = \frac{1}{2}\frac{\mathrm{d}}{\mathrm{d}t}\|\boldsymbol{\Sigma}\|^2 = H_{\text{iso}}(\sigma_{y,0} + H_{\text{iso}}\gamma)\dot{\gamma} \tag{29}$$

it becomes

$$(\sigma_{y,0} + H_{\text{iso}}\gamma)(2G + H_{\text{kin}} + H_{\text{iso}})\dot{\gamma} = 2G[\dot{\mathbf{e}}^{\mathrm{T}}\ \boldsymbol{\Sigma}] \tag{30}$$

Now the idea is to rewrite the differential system formed by Equations (25) and (26)/(30) introducing an integrating function. Accordingly, we set

$$X_0(\gamma) = \begin{cases} \left(1 + \dfrac{H_{\text{iso}}}{\sigma_{y,0}}\gamma\right)^{2G + H_{\text{kin}}/(H_{\text{iso}})} & \text{if } H_{\text{iso}} \neq 0 \\ \exp\left(\dfrac{2G + H_{\text{kin}}}{\sigma_{y,0}}\gamma\right) & \text{if } H_{\text{iso}} = 0 \end{cases} \tag{31}$$

noting that such a function is continuous for fixed γ and $H_{\text{iso}} \to 0$. Multiplying Equation (25) by $X_0(\gamma)$, we have

$$\frac{\mathrm{d}}{\mathrm{d}t}[\boldsymbol{\Sigma}X_0(\gamma)] = 2G\dot{\mathbf{e}}X_0(\gamma) \tag{32}$$

At this stage, defining a new $(n+1)$-dimensional *generalized stress vector* $\mathbf{X}$ as

$$\mathbf{X} = \begin{pmatrix} X_0\boldsymbol{\Sigma} \\ X_0 \end{pmatrix} = \begin{pmatrix} \mathbf{X}^s \\ X_0 \end{pmatrix} \tag{33}$$

from (32) we obtain

$$\dot{\mathbf{X}}^s = 2GX_0\dot{\mathbf{e}} \tag{34}$$

We now search a similar differential equation for the last component X_0 of $\mathbf{X}$. Taking the derivative of $X_0(\gamma)$, we have

$$\dot{X_0} = \frac{\mathrm{d}}{\mathrm{d}t}X_0(\gamma(t)) = (2G + H_{\mathrm{kin}})\frac{X_0}{\sigma_{y,0} + H_{\mathrm{iso}}\gamma}\dot{\gamma} \tag{35}$$

From (35) and (30) we obtain

$$\begin{aligned} \dot{X_0} &= \frac{2G + H_{\mathrm{kin}}}{\sigma_{y,0}^2(2G + H_{\mathrm{kin}} + H_{\mathrm{iso}})}\frac{X_0}{(1 + H_{\mathrm{iso}}/(\sigma_{y,0}\gamma)^2)}[2G\dot{\mathbf{e}}^{\mathrm{T}} \;\; \boldsymbol{\Sigma}] \\ &= \frac{2G + H_{\mathrm{kin}}}{\sigma_{y,0}^2(2G + H_{\mathrm{kin}} + H_{\mathrm{iso}})}X_0^{-2H_{\mathrm{iso}}/(2G+H_{\mathrm{kin}})}[2G\dot{\mathbf{e}}^{\mathrm{T}} \;\; \mathbf{X}^s] \end{aligned} \tag{36}$$

Introducing the position

$$\chi = \chi(X_0) = \frac{2G + H_{\mathrm{kin}}}{\sigma_{y,0}^2\,(2G + H_{\mathrm{kin}} + H_{\mathrm{iso}})}X_0^{-2H_{\mathrm{iso}}/(2G+H_{\mathrm{kin}})} \tag{37}$$

and, recalling Equation (26), we have

$$\dot{X_0} = 0 \qquad \text{elastic phase} \tag{38}$$

$$\dot{X_0} = 2G\chi\dot{\mathbf{e}}^{\mathrm{T}}\mathbf{X}^s \qquad \text{plastic phase} \tag{39}$$

Accordingly, Equations (34) and (38)/(39) provide a system for the generalized stress vector $\mathbf{X}$

$$\dot{\mathbf{X}} = \mathbb{A}\mathbf{X} \tag{40}$$

where the matrix $\mathbb{A}$ depends on the actual phase

$$\mathbb{A} = 2G\begin{pmatrix} 0_{n\times n} & \dot{\mathbf{e}} \\ 0_{1\times n} & 0 \end{pmatrix} \qquad \text{elastic phase} \tag{41}$$

$$\mathbb{A} = 2G\begin{pmatrix} 0_{n\times n} & \dot{\mathbf{e}} \\ \chi\dot{\mathbf{e}}^{\mathrm{T}} & 0 \end{pmatrix} \qquad \text{plastic phase} \tag{42}$$

Therefore, the original problem, represented by Equations (3)–(10), has been substituted by a new one, where the relative stress $\boldsymbol{\Sigma}$ and the plastic rate γ are now represented in the form

of vector $\mathbf{X}$. The main advantage of the new form is the quasi linearity, both in the elastic and in plastic phase.

As an example, let us consider the model with no isotropic hardening ($H_{\text{iso}} = 0$). Due to Equations (37) and (42), it is then immediate to check that $\mathbb{A}$ depends only on $\dot{\mathbf{e}}$. This means that, if $\dot{\mathbf{e}}$ is constant in a certain time interval, $\mathbb{A}$ holds the same property: under such a hypothesis the solution of system (40) is known and the problem can be solved *exactly*.

However, in the general case, the matrix $\mathbb{A}$ depends on $\mathbf{X}$, and in this sense we say that the problem is quasi-linear. Anyway, the partial linearity arising in the problem is indeed of great value, allowing us to numerically approximate its solution with excellent results.

4.1. Time-continuous on–off switch

To properly convert the original problem in an equivalent but new differential algebraic format, we also need to introduce an elastic–plastic phase determination criteria expressed in the new generalized stress environment.

For a given phase to be plastic, we need to fulfill the following two conditions:

(i) The relative stress $\boldsymbol{\Sigma}$ must be on the yield surface

$$\|\mathbf{X}^s\|^2 = \|\boldsymbol{\Sigma}\|^2 X_0^2 = (\sigma_{y,0} + H_{\text{iso}}\gamma)^2 X_0^2 = \sigma_{y,0}^2 X_0^{2(H_{\text{iso}}+H_{\text{kin}}+2G)/(2G+H_{\text{kin}})} \tag{43}$$

(ii) The direction of the strain rate $\dot{\mathbf{e}}$ must be outward with respect to the yield surface

$$\boldsymbol{\Sigma}^{\mathrm{T}}\dot{\mathbf{e}} > 0 \quad \Leftrightarrow \quad (\mathbf{X}^s)^{\mathrm{T}}\dot{\mathbf{e}} > 0 \tag{44}$$

If such two conditions are not satisfied, the step is elastic.

5. NUMERICAL ALGORITHM

Besides the position introduced during the discussion of the return map method, we approximate the strain as a linear function in each time sub interval and, for simplicity, we consider the initial values of γ, e^p and $\boldsymbol{\alpha}$ to be zero, so that the initial generalized stress vector is

$$\mathbf{X}_0 = \begin{pmatrix} \mathbf{X}_0^s \\ X_0 \end{pmatrix} = \begin{pmatrix} \boldsymbol{\Sigma}_0 \\ 1 \end{pmatrix} \tag{45}$$

Clearly, the initial values of the relative stress and the deviatoric strain must be consistent with the governing Equations (3)–(10).

The evolution of $\mathbf{X}$ is governed by the dynamical law (40) with matrix $\mathbb{A}$ given by (41) or (42). Owing to the piecewise linearity of the strain path, $\dot{\mathbf{e}}$ is constant in each single time interval. Unluckily, due to the presence of χ in (42), this is not true for matrix $\mathbb{A}$; the scalar χ is a function of X_0, and so of $\mathbf{X}$, as shown in Equation (37). Therefore, we approximate the solution of the dynamical law (40) considering χ constant in each single time step. Under such an additional hypothesis, the matrix $\mathbb{A}$ is constant in both phases, and so the evolution of Equation (40) is well known to be

$$\mathbf{X}_{n+1} = \exp[\mathbb{A}_n \Delta t]\mathbf{X}_n \tag{46}$$

where $\Delta t = t_{n+1} - t_n$. Defining the vector $\Delta\mathbf{e} = \mathbf{e}_{n+1} - \mathbf{e}_n$, we observe that the matrix $\mathbb{A}_n \Delta t$ is equal to the matrix (41) or (42) after substituting $\dot{\mathbf{e}}$ with $\Delta\mathbf{e}$.

Hence, given the initial value $\mathbf{X}_n$, $\mathbf{X}_{n+1}$ can be now calculated as

$$\mathbf{X}_{n+1} = \bar{\mathbb{G}}\mathbf{X}_n \tag{47}$$

The matrix $\bar{\mathbb{G}}$ is the exponential appearing in (46), which is

$$\bar{\mathbb{G}}_e = \begin{pmatrix} \mathbb{I} & 2G\Delta\mathbf{e} \\ 0 & 1 \end{pmatrix} \tag{48}$$

in the elastic phase, and

$$\bar{\mathbb{G}}_p = \begin{pmatrix} \mathbb{I} + \left[\dfrac{(a-1)}{\|\Delta\mathbf{e}\|^2}\right]\Delta\mathbf{e}\Delta\mathbf{e}^{\mathrm{T}} & \dfrac{b}{\sqrt{\chi}}\dfrac{\Delta\mathbf{e}}{\|\Delta\mathbf{e}\|} \\ b\sqrt{\chi}\,\dfrac{\Delta\mathbf{e}^{\mathrm{T}}}{\|\Delta\mathbf{e}\|} & a \end{pmatrix} \tag{49}$$

in the plastic one. The scalars a and b are

$$a = \cosh\left(2G\sqrt{\chi}\|\Delta\mathbf{e}\|\right) \tag{50}$$

$$b = \sinh\left(2G\sqrt{\chi}\|\Delta\mathbf{e}\|\right) \tag{51}$$

while χ is given by (37) calculated in X_n^0, i.e. the last component of $\mathbf{X}_n$. Such a choice of χ is not only natural (we take its value at the start of the step) but also of simple application. More accurate and performing choices could be introduced, perhaps requiring some implicit calculation instead of the direct matrix product (47).

In conclusion, at every time step the numerical scheme is as follows:

(i) suppose the step to be elastic and compute trial values following an elastic law

$$\mathbf{X}_{n+1}^{TR} = \bar{\mathbb{G}}_e\mathbf{X}_n \tag{52}$$

where the matrix $\bar{\mathbb{G}}_e$ is given by (48). If the trail solution is admissible, i.e.

$$\|\mathbf{X}_{n+1}^{TR}\| \leqslant \sigma_{y,0}(X_{0,n+1}^{TR})^{(H_{\mathrm{iso}}+H_{\mathrm{kin}}+2G)/(2G+H_{\mathrm{kin}})} \tag{53}$$

then the variable values at the time step t_{n+1} are taken as the trial one just calculated.

(ii) If the trail solution is non-admissible, i.e. Equation (53) is violated, then the step is plastic. Being $\dot{\mathbf{e}}$ constant in each sub time interval, this means that the step can be divided into two parts: an elastic deformation followed by a plastic one. We represent with a scalar $\alpha \in [0, 1)$ the elastic time proportion of the step; for example $\alpha = \frac{1}{2}$ means that the stress evolution is of elastic kind for the first half of the time interval, and plastic in the rest. Simple geometrical considerations allow us to compute α; without discussing the details, the obtained value is

$$\alpha = \frac{\sqrt{C^2 - DM} - C}{D} \tag{54}$$

where

$$C = 2GX_{0,n}(\mathbf{X}_n^s)^{\mathrm{T}}\Delta\mathbf{e}$$

$$D = (2GX_{0,n}\|\Delta\mathbf{e}\|)^2$$

$$M = \|\mathbf{X}_n^s\|^2 - \sigma_{y,0}^2(X_{0,n})^{2\varphi} \tag{55}$$

$$\varphi = \frac{2G + H_{\mathrm{kin}} + H_{\mathrm{iso}}}{2G + H_{\mathrm{kin}}}$$

Computed α, $\mathbf{X}_{n+1}$ is updated in two steps.

– Calculate $\mathbf{X}_{n+1}^{TR}$ following an elastic law:

$$\mathbf{X}_{n+1}^{TR} = \bar{\mathbb{G}}_e\mathbf{X}_n \tag{56}$$

with $\bar{\mathbb{G}}_e$ still given by (48), *but* where $\Delta\mathbf{e} = \alpha(\mathbf{e}_{n+1} - \mathbf{e}_n)$ instead of $\Delta\mathbf{e} = (\mathbf{e}_{n+1} - \mathbf{e}_n)$.

– Calculate $\mathbf{X}_{n+1}$ evolving from the new initial data $\mathbf{X}_{n+1}^{TR}$ following a plastic law:

$$\mathbf{X}_{n+1} = \bar{\mathbb{G}}_p\mathbf{X}_{n+1}^{TR} \tag{57}$$

with $\bar{\mathbb{G}}_p$ given by (48), where $\Delta\mathbf{e} = (1-\alpha)(\mathbf{e}_{n+1} - \mathbf{e}_n)$ instead of $\Delta\mathbf{e} = (\mathbf{e}_{n+1} - \mathbf{e}_n)$. Observe that in such a framework purely plastic steps are simply those where the time proportion of elastic phase α is zero.

(iii) Whenever needed, calculate the relative stress and backstress as:

$$\boldsymbol{\Sigma} = \frac{\mathbf{X}^s}{X_0} \tag{58}$$

$$\boldsymbol{\alpha} = H_{\mathrm{kin}}\mathbf{e}^p = H_{\mathrm{kin}}\frac{2G\mathbf{e} - \boldsymbol{\Sigma}}{2G + H_{\mathrm{kin}}} \tag{59}$$

The first one is immediately obtained from the definition of $\mathbf{X}$, while the second one follows from (4) and (5), observing that $\boldsymbol{\alpha} = H_{\mathrm{kin}}\mathbf{e}^p$.

(iv) Finally, at the end of each step update the constant $\chi = \chi(X_{0,n+1})$ used for the calculation of the matrix $\bar{\mathbb{G}}_p$.

Remark 3

Owing to the approximation introduced assuming χ constant in each time step, during a plastic step Equation (43) is not exactly enforced (while in the radial return map method this is fulfilled). However, this discrepancy seems to resolve in very small numerical errors as shown in the examples that follow. A cure to this could be a radial projection of the solution on the yield surface at the end of each time step; anyway we observed that introducing such a correction does not change significantly the solution. In the future it could be worthed to find an approximating scheme of Equation (40), which exactly satisfies the yield condition during the plastic phase without the need of a radial projection.

5.1. Tangent matrix

The algorithmically consistent tangent matrix can be obtained properly linearizing the time-discrete procedure. From the definition of the generalized stress vector $\mathbf{X}$ we get

$$\frac{\partial \mathbf{X}^s}{\partial \mathbf{e}} = \boldsymbol{\Sigma}\frac{\partial X_0}{\partial \mathbf{e}} + X_0\frac{\partial \boldsymbol{\Sigma}}{\partial \mathbf{e}} \tag{60}$$

hence

$$\frac{\partial \boldsymbol{\Sigma}}{\partial \mathbf{e}} = \frac{1}{X_0}\left(\frac{\partial \mathbf{X}^s}{\partial \mathbf{e}} - \boldsymbol{\Sigma}\frac{\partial X_0}{\partial \mathbf{e}}\right) \tag{61}$$

For the elastic phase we immediately have

$$\frac{\partial \mathbf{X}^s}{\partial \mathbf{e}} = 2GX_0\mathbb{I} \tag{62}$$

$$\frac{\partial X_0}{\partial \mathbf{e}} = \mathbf{0} \tag{63}$$

while in the plastic phase the result is far more complicated and can be found in the Appendix.

For the total stress, Equation (5) provides

$$\frac{\partial \mathbf{s}}{\partial \mathbf{e}} = \frac{\partial \boldsymbol{\Sigma}}{\partial \mathbf{e}} + \frac{\partial \boldsymbol{\alpha}}{\partial \mathbf{e}} \tag{64}$$

and, recalling also Equation (59), it becomes

$$\frac{\partial \mathbf{s}}{\partial \mathbf{e}} = \frac{2G}{2G + H_{\text{kin}}}\frac{\partial \boldsymbol{\Sigma}}{\partial \mathbf{e}} + \frac{2GH_{\text{kin}}}{2G + H_{\text{kin}}}\mathbb{I} \tag{65}$$

We also have

$$\frac{\partial \mathbf{s}}{\partial \boldsymbol{\varepsilon}} = \frac{\partial \mathbf{s}}{\partial \mathbf{e}}\frac{\partial \mathbf{e}}{\partial \boldsymbol{\varepsilon}} = \frac{\partial \mathbf{s}}{\partial \mathbf{e}}\mathbb{I}_{\text{dev}} \tag{66}$$

where $\mathbb{I}_{\text{dev}}$ was already defined in (20). Taking into account the volumetric part of the stress, from Equations (1) to (3), we obtain the tangent matrix

$$\frac{\partial \boldsymbol{\sigma}}{\partial \boldsymbol{\varepsilon}} = \frac{\partial \mathbf{s}}{\partial \boldsymbol{\varepsilon}} + K(\mathbf{i}\,\mathbf{i}^{\mathrm{T}}) \tag{67}$$

Joining statements (61), (65), (66) and (67) we obtain

$$\frac{\partial \boldsymbol{\sigma}}{\partial \boldsymbol{\varepsilon}} = \frac{2G}{X_0(2G + H_{\text{kin}})}\left(\frac{\partial \mathbf{X}^s}{\partial \mathbf{e}} - \boldsymbol{\Sigma}\frac{\partial X_0}{\partial \mathbf{e}}\right)\mathbb{I}_{\text{dev}} + \frac{2GH_{\text{kin}}}{2G + H_{\text{kin}}}\mathbb{I}_{\text{dev}} + K(\mathbf{i}\,\mathbf{i}^{\mathrm{T}}) \tag{68}$$

which in the elastic case simplifies to the usual

$$\frac{\partial \boldsymbol{\sigma}}{\partial \boldsymbol{\varepsilon}} = 2G\mathbb{I}_{\text{dev}} + K(\mathbf{i}\,\mathbf{i}^{\mathrm{T}}) \tag{69}$$

and in the plastic one can be calculated substituting the matrix $\partial \mathbf{X}^s/\partial \mathbf{e}$ and the vector $\partial X_0/\partial \mathbf{e}$, which are found in the appendix.

6. NUMERICAL TESTS

We now investigate the validity of the new algorithm through some numerical tests, comparing the results with those obtained through the classical radial return map method. This section is divided in two parts.

In the first one, we test both algorithms on five different pointwise stress–strain load histories, while in the second part we compare the two algorithm performances on a classical initial boundary value problem.

The point-wise numerical tests were performed with the aid of the CE-Driver [14], while the boundary value problem was completed with the aid of the finite element code FEAP [15].

6.1. Point-wise stress–strain tests

Initially, we tested the algorithms on two simple load histories, reproducing a pure tension test and a pure torsion test; the numerical solutions obtained from both methods were extremely close and therefore we omit to present the relative results.

We then considered three biaxial non-proportional load histories, graphically represented in Figure 1. The loading histories are obtained assuming to control the two strain components indicated in the figure and requiring that all the stress components not corresponding to the two controlled strain components are identically equal to zero. In particular, in the three biaxial problems we control the following strain components:

$$\text{Problem 1:} \quad \varepsilon_{11}\ \varepsilon_{12}$$

$$\text{Problem 2:} \quad \varepsilon_{11}\ \varepsilon_{22}$$

$$\text{Problem 3:} \quad \varepsilon_{11}\ \varepsilon_{12}$$

The material constants used were

$$E = 1000\ \text{MPa}, \quad \nu = 0.3$$

$$H_{\text{kin}} = 300\ \text{MPa}, \quad H_{\text{iso}} = 300\ \text{MPa}, \quad \sigma_{y,0} = 5000\ \text{MPa}$$

where the Young's Modulus E and the Poisson ratio ν uniquely determine the constants

$$K = \frac{E}{3(1-2\nu)} \quad G = \frac{E}{2(1+\nu)} \tag{70}$$

Lacking the analytical solution of the problems under investigation, we computed the numerical solutions with a very fine time interval, corresponding to 1000 steps per second [$\mathrm{d}t = 0.001$ s]; such 'exact' solutions were compared with the 'numerical' ones, corresponding to 20 steps per second [$\mathrm{d}t = 0.05$ s], i.e. obtained with a more practical discretization.

At a given time t_n we introduced the following relative norm:

$$E_n = \frac{\|\mathbf{v}_n - \bar{\mathbf{v}}_n\|}{\sup_{j\in\{0,1,\ldots,n\}} \|\mathbf{v}_j\|} \tag{71}$$

where $\|\cdot\|$ indicates the usual ℓ^2 vector norm, while $\mathbf{v}_n$ and $\bar{\mathbf{v}}_n$ are vectors, containing, respectively, the 'exact' and the 'numerical' solution at time t_n. The error measure (71)

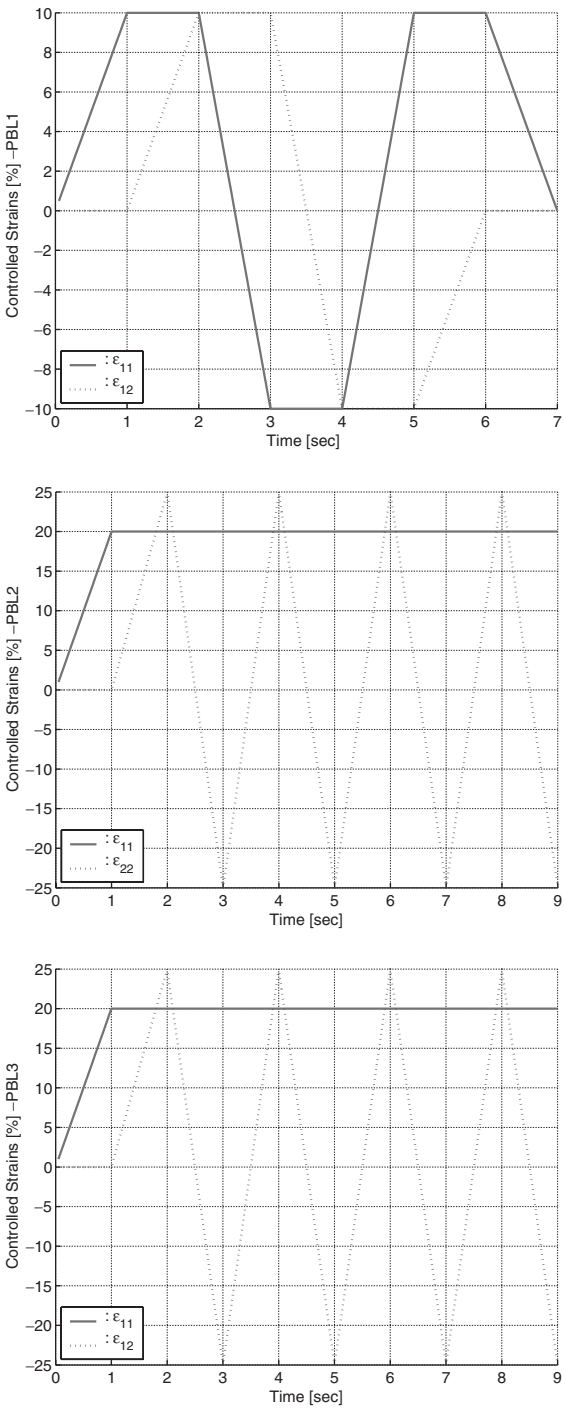

Figure 1. Point-wise stress–strain load histories.

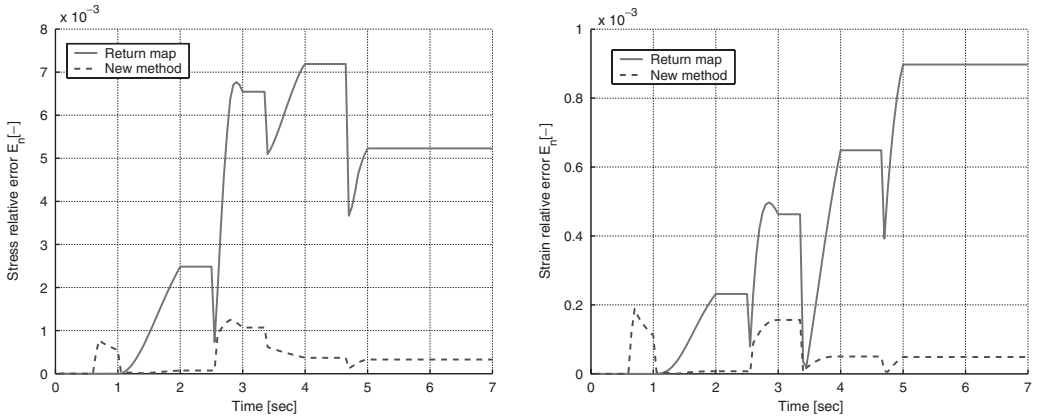

Figure 2. Stress and strain error—Pbl 1.

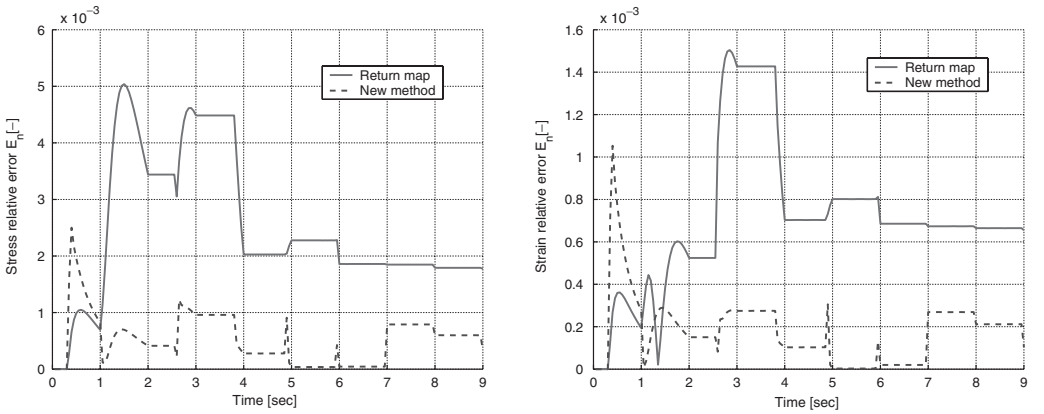

Figure 3. Stress and strain error—Pbl 2.

was used because of the strong variation of the problem solution, which makes inappropriate the use of the classical relative error:

$$\hat{E}_n = \frac{\|\mathbf{v}_n - \bar{\mathbf{v}}_n\|}{\|\mathbf{v}_n\|} \tag{72}$$

Moreover, in the following error, defined as in Equation (71), was evaluated separately for the stress and the strain.

Figures 2–4 report the considered relative errors, respectively, for the first, the second and the third load history. The continuous graph represents the error generated with the radial return map algorithm, while the dashed one is relative to the new method.

The good results obtained with the new algorithm can be immediately appreciated. The radial return map behaves slightly better only in the first part of the tests, while later on the new method behaves much better.

We observed that the new algorithm is very satisfactory also in terms of error behaviour with respect to the time step size. In fact, we solved the three problems with different time

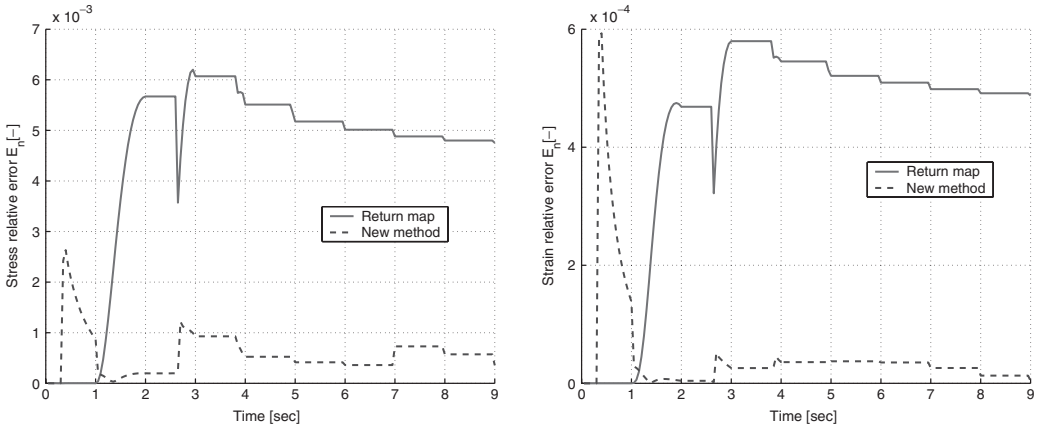

Figure 4. Stress and strain error—Pbl 3.

Table I. Stress total error versus time step size for the first two problems using the new algorithm and the return map algorithm.

Load history	Steps/s	Total error return map ($\times 10^{-2}$)	Total error new algorithm ($\times 10^{-2}$)
1	10	53.27	9.061
1	20	28.49	2.446
1	40	14.40	0.6381
1	80	7.126	0.1618
2	10	131.7	51.51
2	20	66.51	12.86
2	40	33.71	2.829
2	80	16.30	0.5536

step sizes, introducing now a *total error* as the ℓ^1 norm in time of the absolute error:

$$E_T = \sum_{n=1}^{N} \|\mathbf{v}_n - \bar{\mathbf{v}}_n\| \tag{73}$$

where $\mathbf{v}_n$ and $\bar{\mathbf{v}}_n$ are defined as above. Table I reports the stress total error for the first two problems. Apart the undoubtedly lower total error, Table I shows the increased convergence speed of the new method; while the radial return map seems to divide the error by 2 every time we double the number of steps (error goes as h), with the new algorithm the error is instead divided roughly by 4 (error goes as h^2). This aspect is emphasized in Figure 5, where for both methods we plotted the total error versus the number of grid steps in logarithmic scales.

Finally, other numerical tests confirm the following analytic result: *when H_{iso} is set to zero*, the new algorithm is exact. For example, in Figure 6 we plotted the relative error (71) generated by both methods on the first load history with no isotropic hardening and 10 steps per second.

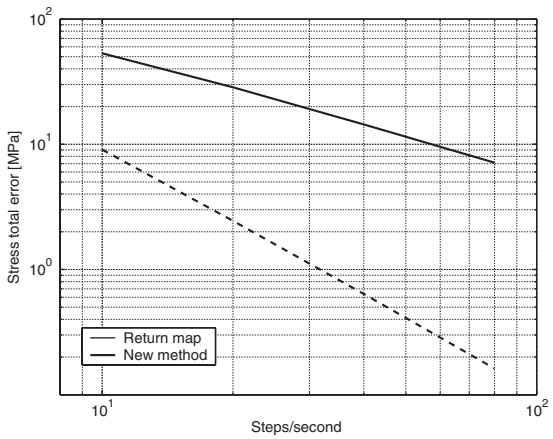

Figure 5. Stress total error versus time step size for the first problem using the new method and the return map.

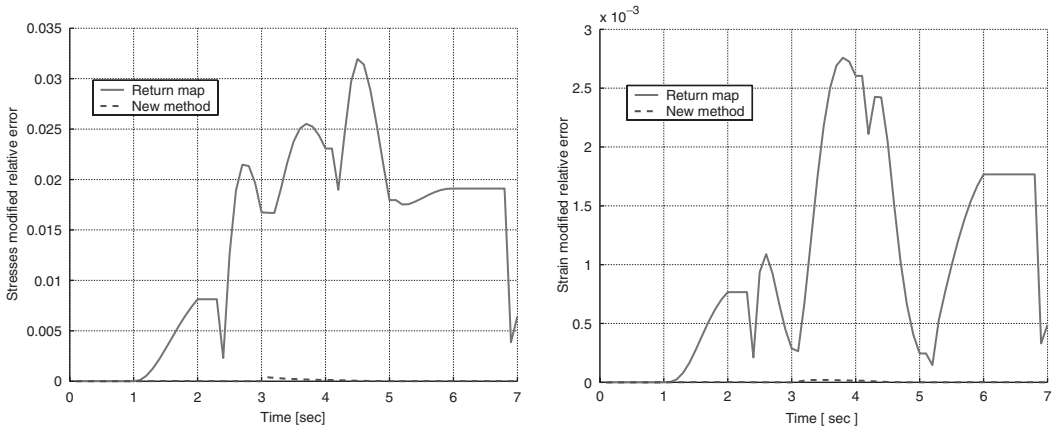

Figure 6. Stress and strain error—Pbl 1 with no isotropic hardening.

6.2. *An initial boundary value problem*

We consider the problem of a three-dimensional perforated strip subject to uniaxial extension [10].

The strip thickness is 1 mm, while its width and height are, respectively, 32 and 20 mm. The hole is in the centre of the strip, and its radius is 5 mm.

In $\mathscr{R}^3$, we describe the material body S as

$$S = \{(x, y, z) \in \mathscr{R}^3 : \ -10 \leqslant x \leqslant 10, \quad -18 \leqslant y \leqslant 18, \quad -0.5 \leqslant z \leqslant 0.5, \quad \sqrt{x^2 + y^2} \geqslant 5\} \tag{74}$$

The material data are

$$E = 70 \text{ MPa}, \qquad \nu = 0.2$$
$$\sigma_{y,0} = 0.8 \text{ MPa}, \quad H_{\text{kin}} = 0 \text{ MPa}, \quad H_{\text{iso}} = 0 \text{ MPa}$$

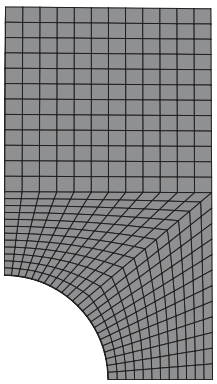

Figure 7. Projection on the $(x–y)$ plane of the mesh used.

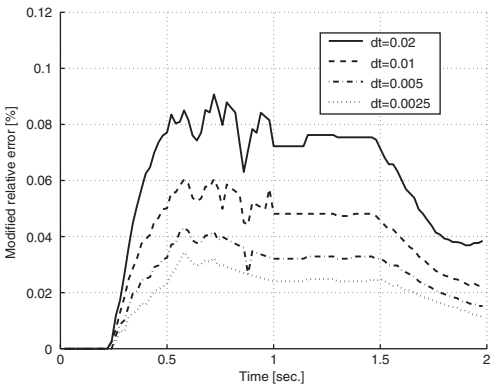

Figure 8. Modified relative difference for the horizontal displacement in $(5,0,0)$ between the new method ($\mathrm{d}t = 0.2$) and the Return map (variable $\mathrm{d}t$).

The two-dimensional projection on the $(x–y)$ plane of the mesh used is presented in Figure 7; note that, due to its symmetries, the problem can be analysed and solved on a quarter of the original domain.

During the numerical experiments, the displacements of the shorter sides ($y = \pm 18$) of the strip are controlled. The history of the problem is composed of a first phase (1 s), in which the strip is stretched imposing a top displacement of $+4$ mm and a second phase (1 s) in which the top displacement is reported to 0 mm.

We solved this boundary value problem both with the new method and the return map, and recorded in both cases the displacements at some particular points of the structure, assuming that such displacements are indicators on how the problem is actually approximated by the numerical methods.

In Figure 8, we plot the modified relative difference for the horizontal (x direction) displacement at the point (5,0,0) between the solution obtained with the new method and the return map. By modified relative difference at time t_n of the above displacement we mean (as already presented in (71))

$$\tilde{E}_n = \frac{|D_n - \bar{D}_n|}{\sup_{j\in\{0,1,\ldots,n\}} |D_j|} \tag{75}$$

where D_n is the described displacement at time t_n calculated with the new method, while $\bar{D}_n$ is the one obtained with the return map.

The total number of timesteps for new method is fixed equal to 100 ($\mathrm{d}t = 0.02$), while the return map was tested with 100, 200, 400 and 800 timesteps (respectively, $\mathrm{d}t = 0.02, 0.01, 0.005, 0.0025$).

It can be immediately noticed from Figure 8 that the modified relative difference converges to zero as the number of steps used for the return map increases. If we further increase the return map steps (we tested up to a total of 2000) the aforementioned convergence continues, while refining the new method time grid does not lead to significant differences. This means that the displacement given by the return map converges, as the number of timesteps increase,

to the value calculated via the new method with 100 timesteps. This in agreement with the fact that the new method solution represents, up to a reasonable error, the exact one.

Finally, we observe that similar results were obtained for other points of the structure.

7. CONCLUSIONS

We presented and examined in detail a new numerical method for the resolution of the associative von-Mises elasto-plastic constitutive law with linear kinematic and isotropic hardening, comparing its performances with those of the well established radial return map algorithm. The comparisons were performed mainly via purely constitutive pointwise tests on different stress–strain load histories, and an initial boundary value problem. The numerical tests clearly suggest the following:

- The new scheme is exact in the case of materials without isotropic hardening. Numerical tests on a classical boundary value problem show that this aspect leads to a considerably better performance when compared to the return map.
- When isotropic hardening is introduced, the new method is no more exact but it still retains a better performance on all the computed numerical tests. Moreover, the error seems to holds quadratic convergence, against the linear one of the return map.

On the other side, the following issues are still open

- Properties of accuracy and stability are still to be rigorously addressed.
- It is not trivial the extension to more general elasto-plastic constitutive models, like non linear hardening or non-spherical yield surfaces.

APPENDIX A

In this section, we present the tangent matrices of the generalized stress vector addressed in (61), and compare the new method here described with other approaches also based on an exact integration of the problem.

A.1. Tangent matrix for the generalized stress

In this section we present the tangent matrix $\partial \mathbf{X}^s/\partial \mathbf{e}$ and tangent vector $\partial X_0/\partial \mathbf{e}$ for plastic phases, which, from Equation (68), provide the tangent matrix $\partial \boldsymbol{\sigma}/\partial \boldsymbol{\varepsilon}$ of the new algorithm during plastic or mixed elasto-plastic steps.

Remembering that purely plastic steps are a particular case within the range of mixed ones (see Section 5), we start analysing the latter. We have, from (56)–(57),

$$\mathbf{X}_{n+1} = \bar{\mathbb{G}}_p \bar{\mathbb{G}}_e \mathbf{X}_n = \mathbb{G}_p((1-\alpha)\Delta\mathbf{e})\mathbb{G}_e(\alpha\Delta\mathbf{e})\mathbf{X}_n \tag{A1}$$

where the matrices above are given by (48)–(49) and $\alpha = \alpha(\Delta\mathbf{e})$ is the 'elastic step proportion' defined in (54). Consequently, following basic derivation rules, we have for mixed steps

$$\frac{\partial \mathbf{X}_{n+1}}{\partial \mathbf{e}} = [\tilde{\mathbb{A}}_1 + \tilde{\mathbb{A}}_2 + \tilde{\mathbb{A}}_3 + \tilde{\mathbb{A}}_4]\mathbf{X}_n \tag{A2}$$

where the third-order tensors

$$\begin{aligned}
\tilde{\mathbb{A}}_1 &= \frac{\partial \mathbb{G}_p}{\partial \Delta\mathbf{e}}[(1-\alpha)\Delta\mathbf{e}]\mathbb{G}_e(\alpha\Delta\mathbf{e}) \\
\tilde{\mathbb{A}}_2 &= \frac{\partial \mathbb{G}_p}{\partial \alpha}[(1-\alpha)\Delta\mathbf{e}]\frac{\mathrm{d}\alpha}{\mathrm{d}\Delta\mathbf{e}}(\Delta\mathbf{e})\mathbb{G}_e(\alpha\Delta\mathbf{e}) \\
\tilde{\mathbb{A}}_3 &= \mathbb{G}_p[(1-\alpha)\Delta\mathbf{e}]\frac{\partial \mathbb{G}_e}{\partial \Delta\mathbf{e}}(\alpha\Delta\mathbf{e}) \\
\tilde{\mathbb{A}}_4 &= \mathbb{G}_p[(1-\alpha)\Delta\mathbf{e}]\frac{\partial \mathbb{G}_e}{\partial \alpha}(\alpha\Delta\mathbf{e})\frac{\mathrm{d}\alpha}{\mathrm{d}\Delta\mathbf{e}}(\Delta\mathbf{e})
\end{aligned} \tag{A3}$$

From Equation (A2) we can immediately derive $\partial \mathbf{X}^s_{n+1}/\partial\mathbf{e}$ (first six components) and $\partial \mathbf{X}_{0,n+1}/\partial\mathbf{e}$ (last component); in order to obtain the classical tangent matrix, the obtained equations must be finally expressed as a linear function of the strain derivation vector instead of in the form (A2), which is expressed as a linear function of $\mathbf{X}_n$. Doing so, we finally obtain that for mixed steps

$$\frac{\partial \mathbf{X}^s}{\partial \mathbf{e}} = (\mathbb{A}_1 + \mathbb{A}_2 + \mathbb{A}_3 + \mathbb{A}_4) \tag{A4}$$

$$\frac{\partial \mathbf{X}_0}{\partial \mathbf{e}} = (\mathbf{b}_1 + \mathbf{b}_2 + \mathbf{b}_3 + \mathbf{b}_4) \tag{A5}$$

where the matrices $\mathbb{A}$ and vectors $\mathbf{b}$ are described below without addressing the calculations.

For purely plastic steps, being α constantly equal to zero, we instead obtain the shorter formulation

$$\frac{\partial \mathbf{X}^s}{\partial \mathbf{e}} = \mathbb{A}_1 \tag{A6}$$

$$\frac{\partial \mathbf{X}_0}{\partial \mathbf{e}} = \mathbf{b}_1 \tag{A7}$$

We start introducing (see again (54) for M, D, C in each step) the $v = \mathrm{d}\alpha/\mathrm{d}\Delta\mathbf{e}$ vector

$$\begin{aligned}
v &= \phi_1 \frac{\mathrm{d}C}{\mathrm{d}\Delta\mathbf{e}} + \phi_2 \frac{\mathrm{d}D}{\mathrm{d}\Delta\mathbf{e}} \\
\phi_1 &= \frac{1}{D}\left(\frac{C}{\sqrt{C^2 - DM}} - 1\right) \\
\phi_2 &= -\frac{1}{D^2}\left(\frac{DM}{2\sqrt{C^2 - DM}} + \sqrt{C^2 - DM} - C\right) \\
\frac{\mathrm{d}C}{\mathrm{d}\Delta\mathbf{e}} &= 2GX_{0,n}\mathbf{X}^s_n \\
\frac{\mathrm{d}D}{\mathrm{d}\Delta\mathbf{e}} &= 2(2GX_{0,n})^2\Delta\mathbf{e}
\end{aligned} \tag{A8}$$

Let the scalars

$$\begin{aligned} a &= \cosh\left(2G(1-\alpha)\sqrt{\chi}\|\Delta\mathbf{e}\|\right) \\ b &= \sinh\left(2G(1-\alpha)\sqrt{\chi}\|\Delta\mathbf{e}\|\right) \\ s &= \frac{\Delta\mathbf{e}\cdot\mathbf{X}_n^s}{\|\Delta\mathbf{e}\|} \\ k &= 2G(1-\alpha)\sqrt{\chi} \\ \tilde{k} &= -2G\sqrt{\chi}\|\Delta\mathbf{e}\| \end{aligned} \tag{A9}$$

and the matrices

$$\mathbb{M}_1 = s\left(kb - 2\frac{a-1}{\|\Delta\mathbf{e}\|}\right)\left[\frac{\Delta\mathbf{e}\Delta\mathbf{e}^{\mathrm{T}}}{\|\Delta\mathbf{e}\|^2}\right] + \frac{(a-1)s}{\|\Delta\mathbf{e}\|}\mathbb{I} + \frac{a-1}{\|\Delta\mathbf{e}\|}\left[\frac{\Delta\mathbf{e}\mathbf{X}_n^{s\mathrm{T}}}{\|\Delta\mathbf{e}\|}\right] \tag{A10}$$

$$\mathbb{M}_2 = \left(ka - \frac{b}{\|\Delta\mathbf{e}\|}\right)\left[\frac{\Delta\mathbf{e}\Delta\mathbf{e}^{\mathrm{T}}}{\|\Delta\mathbf{e}\|^2}\right] + \frac{b}{\|\Delta\mathbf{e}\|}\mathbb{I} \tag{A11}$$

We then have, for the matrices in (A4),

$$\begin{aligned} \mathbb{A}_1 &= \mathbb{M}_1 + \frac{X_{0,n}}{\sqrt{\chi}}\mathbb{M}_2 \\ \mathbb{A}_2 &= \tilde{k}\left(bs + \frac{a}{\sqrt{\chi}}X_{0,n}\right)\left[\frac{\Delta\mathbf{e}v^{\mathrm{T}}}{\|\Delta\mathbf{e}\|}\right] \\ \mathbb{A}_3 &= 2G\alpha X_{0,n}\left[\mathbb{I} + (a-1)\frac{\Delta\mathbf{e}\Delta\mathbf{e}^{\mathrm{T}}}{\|\Delta\mathbf{e}\|^2}\right] \\ \mathbb{A}_4 &= 2GaX_{0,n}\begin{bmatrix}\Delta\mathbf{e} & v^{\mathrm{T}}\end{bmatrix} \end{aligned} \tag{A12}$$

and for the row vectors in (A5)

$$\begin{aligned} \mathbf{b}_1 &= \sqrt{\chi}\,\mathbf{X}_n^{s\mathrm{T}}\mathbb{M}_2 + kbX_{0,n}\frac{\Delta\mathbf{e}^{\mathrm{T}}}{\|\Delta\mathbf{e}\|} \\ \mathbf{b}_2 &= \tilde{k}(as\sqrt{\chi} + bX_{0,n})v^{\mathrm{T}} \\ \mathbf{b}_3 &= 2G\alpha bX_{0,n}\sqrt{\chi}\frac{\Delta\mathbf{e}^{\mathrm{T}}}{\|\Delta\mathbf{e}\|} \\ \mathbf{b}_4 &= 2GbX_{0,n}\sqrt{\chi}\|\Delta\mathbf{e}\|v^{\mathrm{T}} \end{aligned} \tag{A13}$$

where a column vector after a matrix, or a row vector before, represents a matrix–vector product as usual. The structure here given is the same we actually reproduced during the implementation.

Remark 4
Let us restrict ourselves to the case of purely plastic steps without isotropic hardening. Then, it can be checked that, when $\|\Delta\mathbf{e}\| \to 0$, our tangent matrix (68) converges to the continuous tangent matrix

$$\mathbb{D}_c = K(\mathbf{i}\,\mathbf{i}^{\mathrm{T}}) + 2G\mathbb{I}_{\mathrm{dev}} + 2G\frac{2G}{2G + H_{\mathrm{kin}}}\mathbf{n}^{TR}[\mathbf{n}^{TR}]^{\mathrm{T}} \tag{A14}$$

This is right, because in the purely kinematic hardening case our algorithm is exact and therefore the solution corresponds to the continuous one. On the other side, when $\|\Delta\mathbf{e}\| \neq 0$, the tangent *must* instead be different from the classical continuous one, which does not consider that during a practical implementation the derivative is influenced also by the step initial stress on the yield surface.

In the case of the Return map, this effect is one of the causes of the correction introduced in (17), when compared to the original $\mathbb{D}_c$.

A.2. Comparison with other 'exact' methods

Other approaches based on an exact integration of the problem are present in the literature (see References [3] and [4] but also References [5, 6] or [7]). All the cited references start from the idea proposed by Krieg and Krieg in Reference [3], where the exact solution for the plasticity constitutive strain driven problem with no hardening is found ($\dot{\mathbf{e}}$ piecewise constant). In order to obtain such result, the problem is restricted to the plane $\{\mathbf{s}, \dot{\mathbf{e}}\}$ (which does not vary whenever $\dot{\mathbf{e}}$ is constant) and solved exactly for the angular variable θ, defined by

$$\mathbf{s} \cdot \dot{\mathbf{e}} = \|\mathbf{s}\|\,\|\dot{\mathbf{e}}\| \cos\theta \tag{A15}$$

Although the method proposed in Reference [3] and the one investigated here are clearly different, the Krieg and Krieg approach can be recovered also in the settings of the present paper. This can be done restricting the problem to the aforementioned plane and solving the deriving equation with substitution (A15) instead of using an integration factor. In fact letting $H_{\mathrm{kin}} = H_{\mathrm{iso}} = 0$, Equation (25) becomes

$$\dot{\mathbf{s}} + \frac{2G}{\sigma_{y,0}}\mathbf{s}\dot{\gamma} = 2G\dot{\mathbf{e}} \tag{A16}$$

which multiplied (scalar product) by $\dot{\mathbf{e}}$ and $\mathbf{s}$, respectively, gives the system

$$\begin{aligned} [\dot{\mathbf{s}} \cdot \dot{\mathbf{e}}] + \frac{2G}{\sigma_{y,0}}[\mathbf{s} \cdot \dot{\mathbf{e}}]\dot{\gamma} &= 2G\|\dot{\mathbf{e}}\|^2 \\ \dot{\gamma} &= \frac{1}{\sigma_{y,0}}[\mathbf{s} \cdot \dot{\mathbf{e}}] \end{aligned} \tag{A17}$$

which is solvable substituting the second equation in the first and using (A15). It is interesting to observe that the generalization of the method found in Reference [3] to the isotropic hardening case leads to equations which cannot be solved exactly (see Reference [4]), nor have an undergoing structure suggesting an immediate numerical approach. The first statement seems true also for the new method here presented but, although clearly less direct when compared to a more geometrical approach, the use of an integration factor holds the big

advantage of leading to the 'quasi-linear' system (40) which can be approximated numerically with great efficiency and accuracy.

ACKNOWLEDGEMENTS

The authors express their gratitude to Professor Franco Brezzi and Professor Carlo Lovadina of the Pavia Department of Mathematics for their valuable support.

REFERENCES

1. Hong-Ki Hong, Chien-Shan Liu. Internal symmetry in bilinear elastoplasticity. *International Journal for Non-Linear Mechanics* 1999; **34**:279–288.
2. Hong-Ki Hong, Chien-Shan Liu. Internal symmetry in the constitutive model of perfect elastoplasticity. *International Journal of Non-Linear Mechanics* 2000; **35**:447–466.
3. Krieg RD, Krieg DB. Accuracies of numerical solution methods for the elastic-perfectly plastic model. *Journal of Pressure Vessel Technology* (ASME) 1997; **99**:510–515.
4. Yoder PJ, Whirley RG. On the numerical implementation of elastoplastic models. *Journal of Applied Mechanics* (ASME) 1984; **51**:283–288.
5. Montmitonnet P, Gratacos P, Chenot JL. An integration scheme for Prandtl-Reuss elastoplasic constitutive equations. *International Journal for Numerical Methods in Engineering* 1992; **33**:943–961.
6. Ristinmaa M, Tryding J. Exact integration of constitutive equations in elasto-plasticity. *International Journal for Numerical Methods in Engineering* 1993; **36**:2525–2544.
7. Peric D, Wei Z, Owen DRJ. Consistent linearization for the exact stress update of Prandtl-Reuss non-hardening elastoplastic models. *International Journal for Numerical Methods in Engineering* 1996; **39**:1219–1235.
8. Chaboche JL. Constitutive equations for cyclic plasticity and cyclic visco-plasticity. *International Journal of Plasticity* 1989; **5**:247–302.
9. Lubliner J. *Plasticity Theory*. Macmillan: New York, 1990.
10. Simo JC, Hughes TJR. *Computational Inelasticity*. Springer: Berlin, 1998.
11. Simo JC. Topics on the numerical analysis and simulation of plasticity. In: *Handbook of Numerical Analysis*, Ciarlet PG, Lions JL (eds). vol. III. Elsevier: Amsterdam, 1999.
12. Auricchio F, Taylor RL. Two material models for cyclic plasticity: non-linear kinematic hardening and generalized plasticity. *International Journal of Plasticity* 1995; **11**:65–98.
13. Zienkiewicz OC, Taylor RL. *The Finite Element Method*, vol. II. McGraw-Hill: New York (4th edn), 1991.
14. Auricchio F. Ce-driver. *Technical Report*, Dipartimento di Meccanica Strutturale, University of Pavia, 2001. Manual prepared for the European School of Advanced Studies of Seismic Risk Reduction.
15. Taylor RL. A finite-element analysis program. *Technical Report*, University of California at Berkeley, 2000. http://www.ce.berkeley.edu/rlt.

